

Research and Development of Bulk Anisotropic Nanograin Composite Rare Earth Permanent Magnets

Sam Liu¹, Don Lee¹, Mei Qing Huang², Ashil Higgins¹, Yuhui Shen³,
Youngson He³, and Christina Chen¹

¹University of Dayton Magnetics Laboratory, 300 College Park, Dayton, OH 45469, USA

²UES Inc., 4401 Dayton-Xenia RD., Dayton, OH 45432, USA

³FutureTek USA Corporation, 454 Patterson Rd, Dayton, OH 45419, USA

Abstract: Innovative and cost-effective technology for synthesizing bulk anisotropic nanograin composite rare earth magnets has been developed. Using a powder blending technique, $(BH)_{\max}$ of nanograin composite magnets can reach 40 to 50 MGOe, while applying powder coating techniques, $(BH)_{\max} = 45 - 55$ MGOe were achieved. Thus, principal technical difficulties in synthesizing bulk anisotropic nanograin composite magnets are successfully overcome. In addition, it was observed that the magnetically soft phase in a composite magnet could be up to tens of micrometers, or more than 1000 times larger than the upper size limit predicted by the current models of interface exchange coupling, which indicates that further reducing the size of the soft phase and improving its distribution will significantly improve the magnetic performance of nanograin composite magnets.

Key words: nanograin composite magnet, interface exchange coupling, Nd-Fe-B, hard phase, soft phase.

1. Introduction

1.1 Background

Research on nanocomposite rare earth magnets started in 1988 when the Philips group observed that intrinsic coercivity of ~ 3 kOe could be obtained in an annealed melt-spun $\text{Nd}_2\text{Fe}_{14}\text{B}/\text{Fe}_3\text{B}$ alloy powder [1-2]. It is believed that the interface exchange coupling between a magnetically hard phase ($\text{Nd}_2\text{Fe}_{14}\text{B}$) and a magnetically soft phase (Fe_3B) restricts magnetization directions in the soft phase, leading to a smooth demagnetization curve and relatively high coercivity. Extensive research and development of nanocomposite magnets followed in 1990s [3-7]. It was predicted that a very high $(BH)_{\max}$ (up to ~ 100 MGOe) could be reached in this new type of permanent magnet [3,6]. However, the worldwide effort in making high-performance nanocomposite magnets encountered various technical difficulties. As a result, prior to 2002, only isotropic nanocomposite alloy powders or ribbons could be made with $(BH)_{\max}$ up to ~ 20 MGOe. These powders could be further made into bonded magnets with $(BH)_{\max}$ up to ~ 10 MGOe.

1.2. Technical difficulties in making bulk anisotropic nanocomposite magnets

Nanocomposite magnet materials are prepared using either a melt spinning process or a mechanical alloying process. Generally speaking, materials obtained after melt spinning and mechanical alloying are ribbons or powders in an amorphous condition. After annealing at or above the crystallization temperature, a nanograin structure can be formed and isotropic nanograin powders can be obtained.

All conventional rare earth magnet alloys, such as Sm-Co and Nd-Fe-B, contain a minor low-melting-point rare earth-rich phase that is critically important for consolidation. Because a nanocomposite magnet powder, such as $\text{Nd}_2\text{Fe}_{14}\text{B}/\alpha\text{-Fe}$ does not contain a Nd-rich phase, it had been very difficult to make it into bulk nanocomposite magnets with near full density by applying conventional consolidation techniques, such as sintering or hot press. In addition, high-temperature processing, such as sintering, leads to excessive grain growth, which destroys the desired nanograin structure.

It had been also very difficult to make grain alignment and obtain high-performance anisotropic nanocomposite $\text{Nd}_2\text{Fe}_{14}\text{B}/\alpha\text{-Fe}$ or $\text{Nd}_2\text{Fe}_{14}\text{B}/\text{Fe}_3\text{B}$ magnets using conventional technologies. The fine powder magnetic alignment technique could not be used for nanocomposite powders. As opposed to conventional magnet powders, each micron-sized particle of nanocomposite powder contains numerous nanograins that are randomly distributed throughout the particle. Therefore, powder particles containing nanograins cannot be aligned in a magnetic field.

This study was partially sponsored by the US Defense Advanced Research Projects Agency through the US Office of Naval Research under contract N00014-03-01-0636 and through the US Air Force Research Laboratory under contract F33615-01-2-2166, by the US Air Force Research Laboratory under contract F33615-02-D-2299, and by the US Department of Energy under contract DE-FG02-05ER86242

Sam Liu, Phone: (937)229-3272; E-mail: lius@udri.udayton.edu.

On the other hand, the hot deformation technique could not be used to create grain alignment in a nanocomposite $\text{Nd}_2\text{Fe}_{14}\text{B}/\alpha\text{-Fe}$ magnet in which a Nd-rich phase does not exist. The Nd-rich phase in the conventional Nd-Fe-B magnet alloys plays a critical role in hot deformation and texture formation. At the hot deformation temperature, the Nd-rich phase is in a melted condition and serves as a lubricant, which makes the deformation possible without cracks and facilitates the texture formation [8]. Because a nanocomposite $\text{Nd}_2\text{Fe}_{14}\text{B}/\alpha\text{-Fe}$ alloy does not contain a Nd-rich phase, the desired grain alignment could not be created by using the hot deformation process.

2. Novel concepts of the effect of nanograin structure on magnetic properties

A fundamental change takes place in magnetic materials when their grain size is reduced from the micrometer to nanometer range. A convincing example is a $\text{Sm}_2\text{Co}_{17}$ compound. It took more than 10 years for researchers to modify the compositions (by adding Cu, Zr, and extra Sm) and to develop a lengthy and complex sintering and heat-treatment procedure for achieving useful coercivity (> 8 kOe) [9-13]. The procedure consists of high-temperature sintering at $\geq 1200^\circ\text{C}$ for 1 to 2 hours, a solid solution heat treatment at $\sim 1180^\circ\text{C}$ for a few hours, a very long aging period at $\sim 800^\circ\text{C}$ for 20 to 50 hours, followed by slow cooling from 800 to 400°C at 1 to $2^\circ\text{C}/\text{minute}$. The whole procedure takes about three days to complete. These compositional modifications and heat treatments are required to form a fine-scale cellular microstructure in which the cell boundary phase serves as pinning sites for domain wall motion, leading to high coercivity [11,12].

However, if the grain size of $\text{Sm}_2\text{Co}_{17}$ is reduced from micron range to nanometer range, high intrinsic coercivity can be easily developed in the stoichiometric $\text{Sm}_2\text{Co}_{17}$ (without adding extra Sm and Cu, Zr and without long-term aging). In 1991, J. Wecker, et al. [4] obtained 6 kOe after annealing a mechanically alloyed stoichiometric $\text{Sm}_2\text{Co}_{17}$ alloy powder at 700°C for 30 minutes. A few years later, S.K. Chen, et al. [14] obtained 4 kOe after annealing a mechanically alloyed SmCo_{10} alloy powder at 750°C for 20 minutes. More recently, a high coercivity of 15.6 kOe was accomplished at the University of Dayton Magnetism Laboratory after annealing a mechanically alloyed $\text{Sm}_2\text{Co}_{17}$ specimen at 750°C for only 1 minute [15]. The TEM observation did not find the cellular structure in the specimen [16], therefore, the magnetization reversal must be

carried out by other mechanisms rather than domain wall pinning.

Based on novel phenomena observed in magnetic materials having nanograin structure, an innovative coercivity model was proposed [16]. According to this model, high uniaxial magneto-crystalline anisotropy is not only a necessary condition for high coercivity, as it is in magnets having micrometer grains, it is also the sufficient condition for high coercivity in magnets having nanograins. Therefore, high coercivity can be readily obtained for any magnetic materials that have high uniaxial anisotropy, provided that the materials possess nanograin structure.

3. Technology of synthesizing bulk nanocomposite magnets

Since high coercivity could be readily obtained by annealing amorphous stoichiometric $\text{Sm}_2\text{Co}_{17}$ and Nd-poor Nd-Fe-B alloys for only a very short period of time, then developing a new consolidation technology should be possible if these amorphous alloy powders could be compacted into bulk materials at their crystallization temperatures with a very fast speed. This compaction procedure actually combines two processes: (1) consolidating powder particles into a bulk material with near full density, and (2) crystallizing an amorphous alloy and forming the desired nanograin structure. Because the crystallization temperature of an amorphous alloy is not high (around 600 to 650°C for Nd-Fe-B), compacting an amorphous alloy powder at that temperature for a very short time will effectively avoid excessive grain growth, thus, ensuring that the fine nanograin structure can be maintained in a bulk form.

Based on this understanding, an innovative RF rapid inductive hot compaction technology was successfully developed at the University of Dayton in 2002 [17-19]. By applying this consolidation technology, amorphous isotropic nanocomposite $\text{Nd}_2\text{Fe}_{14}\text{B}/\alpha\text{-Fe}$ powder can be compacted into bulk magnets with full density in around 2 minutes, including heating from room temperature, performing the compaction at 600 to 650°C (exactly the crystallization temperature of the amorphous $\text{Nd}_2\text{Fe}_{14}\text{B}/\alpha\text{-Fe}$), and cooling down to $\sim 300^\circ\text{C}$. After the hot compaction, bulk, fully dense, isotropic Nd-Fe-B/ $\alpha\text{-Fe}$ magnets with uniform nanograin structure can be obtained.

Figure 1 compares density values obtained in Nd-Fe-B magnets with various Nd contents by using the RF rapid inductive compaction and conventional hot press. It can be seen that when the conventional hot press is used, the density

values sharply drop when the Nd content is lower than ~13.5 at%, while the density values actually slightly increase when the Nd content is reduced if the rapid inductive compaction is used. Though full density and nanograin structure can be readily obtained in various nanocomposite materials by using this innovative technology, its underlying science is not yet fully understood.

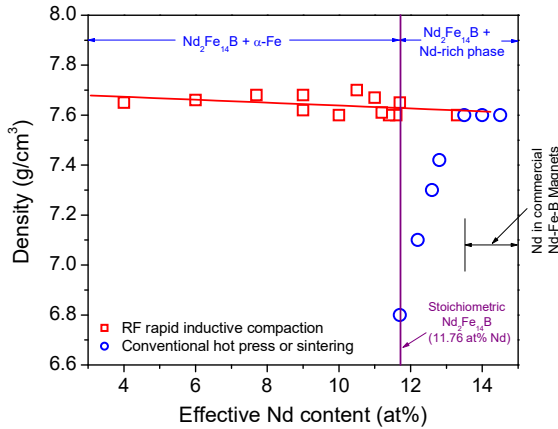


Fig. 1. Density vs. Nd content in Nd-Fe-B magnets synthesized using rapid inductive compaction and conventional hot press.

4. Technologies of synthesizing anisotropic nanograin composite magnets

The inductive hot compaction and the subsequent hot deformation were used to synthesize bulk anisotropic nanograin composite magnets. The experimental conditions were as follows.

The purity levels of the raw materials used in our experiments were: Nd - 95%, Fe > 99%, Co > 99%, and Ga - 99.99 %. The composition of the Fe-B alloy was 20.54 wt% B; 77.72 wt% Fe. The Nd-Fe-B alloys were prepared by vacuum arc melting, followed by melt spinning with a wheel speed of 40 m/s. The ribbons were then crushed to 200 – 300 micrometers. Bulk magnet samples were prepared by a two-step process: RF inductive heating to 600 – 700°C, along with simultaneous compaction under a pressure of $\sim 1.7 \times 10^8$ Pa for a total cycle time of ~ 2 minutes, followed by hot deformation (die upsetting) at 850 – 950°C under a pressure of $\sim 6.9 \times 10^7$ Pa for a total cycle time of 4 – 6 minutes. The typical sample height reduction in the latter step was 71%.

Samples were analyzed using a hysteresisgraph for room temperature magnetic properties, using a 13 mm diameter specimen. SEM, XRD, and TEM were used to characterize particle size, grain alignment, and microstructures.

4.1 Hot compaction and hot deformation of a single Nd-poor Nd-Fe-B powder

After the rapid inductive hot compaction of a single rare earth-poor magnet alloy with the rare earth content in an amount less than the stoichiometric value, a bulk isotropic nanocomposite magnet, such as $\text{Nd}_2\text{Fe}_{14}\text{B}/\alpha\text{-Fe}$, $\text{Nd}_2\text{Fe}_{14}\text{B}/\text{Fe}_3\text{B}$, as well as $\text{Sm}_2(\text{Co,Fe})_{17}/\text{Fe-Co}$, can be readily obtained. However, due to the lack of a rare earth-rich phase in these magnet alloys, it is difficult to create the desired grain alignment in the subsequent hot deformation process.

4.2 Hot compaction and hot deformation of a powder mixture of Nd-poor Nd-Fe-B and Nd-rich Nd-Fe-B

Alternatively, nanocomposite Nd-Fe-B/ α -Fe magnets can be made by hot compacting and hot deforming a mixture of two powders. One powder is a melt-spun Nd-Fe-B that contained a minor Nd-rich phase. The second powder is a melt-spun Nd-Fe-B powder that contained an α -Fe phase. The Nd content in the overall composition can be still lower than that of the chemical stoichiometric $\text{Nd}_2\text{Fe}_{14}\text{B}$. The magnetic performance of nanocomposite magnets prepared using this method demonstrated a significant improvement as compared with those made by processing a single Nd-poor Nd-Fe-B alloy. Under normal conditions, $(\text{BH})_{\text{max}} = 35$ to 40 MGOe can be reached and the best $(\text{BH})_{\text{max}}$ obtained was 45 MGOe.

Figure 2 shows demagnetization curves of a $\text{Nd}_{10.8}\text{Pr}_{0.6}\text{Dy}_{0.2}\text{Fe}_{76.1}\text{Co}_{6.3}\text{Ga}_{0.2}\text{Al}_{0.2}\text{B}_{5.6}$ magnet prepared by hot compacting and hot deforming a powder mixture of a Nd-rich powder of $(\text{Nd,Pr,Dy})_{13.5}(\text{Fe,Co,Ga})_{80.5}\text{B}_6$ and a Nd-poor powder of $\text{Nd}_4\text{Fe}_{90}\text{B}_6$. The α -Fe fraction in the composite magnet is around 3%.

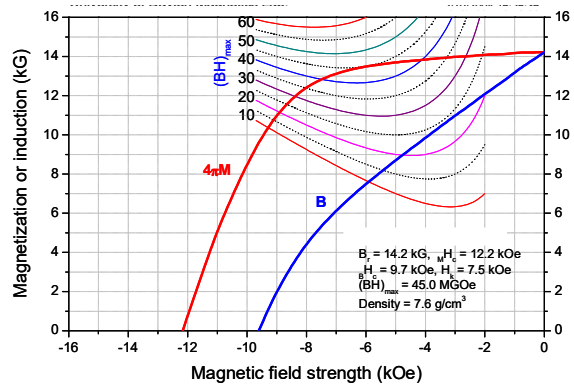


Fig. 2. Demagnetization curves of a bulk anisotropic $\text{Nd}_{10.8}\text{Pr}_{0.6}\text{Dy}_{0.2}\text{Fe}_{76.1}\text{Co}_{6.3}\text{Ga}_{0.2}\text{Al}_{0.2}\text{B}_{5.6}$ magnet with $(\text{BH})_{\text{max}} = 45$ MGOe.

It is important to realize that the desired grain alignment can be created only in the Nd-rich Nd-Fe-B portion during hot deformation. Therefore,

the magnet comprises an anisotropic portion and an isotropic portion.

It was observed that when the Nd content in the Nd-poor alloy (the alloy comprises an α -Fe phase) is decreased, the magnetic performance of the nanocomposite magnet improves. Figure 3 shows the magnetic performance of nanocomposite magnets versus the Nd content in the Nd-poor Nd-Fe-B alloy powder. These nanocomposite magnets have a fixed composition of $\text{Nd}_{11.6}\text{Fe}_{82.4}\text{B}_6$ and were prepared by hot compacting and hot deforming a powder mixture of a Nd-rich alloy powder of $\text{Nd}_{13.5}\text{Fe}_{80.5}\text{B}_6$ and one of the Nd-poor alloy powders with various Nd contents. It can be seen that when the Nd content in the Nd-poor alloy powder is reduced, the performance of nanocomposite $\text{Nd}_{11.6}\text{Fe}_{82.4}\text{B}_6$ magnets is improved and the best $(\text{BH})_{\text{max}}$ is obtained when the Nd content in the Nd-poor alloy is reduced to 4 at%.

This interesting result implies that if the Nd content in the Nd-poor alloy powder is further reduced from 4 at% to 0%, which makes the alloy a pure Fe metal with a very small amount of boron content, further improvement in magnetic performance may be achieved, as shown in Figure 3.

That was exactly what happened in the experiments. A significant advance in magnetic performance was accomplished by hot compacting and hot deforming a powder mixture of a Nd-rich Nd-Fe-B alloy powder and commercial powder particles of α -Fe or Fe-Co, which gives birth to another innovative method for making nanocomposite magnets.

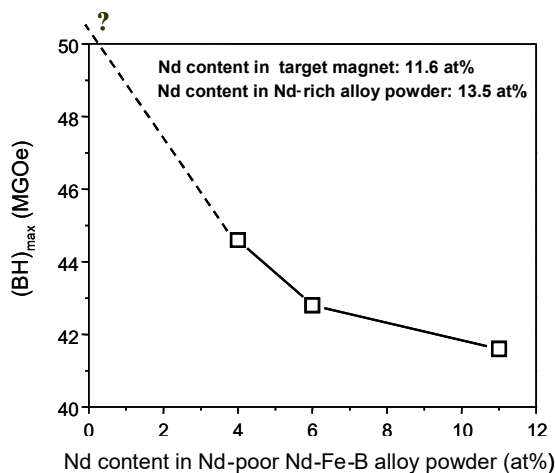


Fig. 3. $(\text{BH})_{\text{max}}$ vs. Nd content in the Nd-poor Nd-Fe-B alloy.

4.3 Hot compaction and hot deformation of a powder mixture of Nd-rich Nd-Fe-B and an α -Fe or Fe-Co powder

This technology was developed by reducing the Nd content in the Nd-poor Nd-Fe-B to zero in the previous technology. Grain alignment can be significantly improved by avoiding the isotropic portion completely. However, the fine α -Fe powder tends to be agglomerated, which decreases the intrinsic coercivity and knee field. $(\text{BH})_{\text{max}}$ values of 40 to 50 MGOe can be reached using this technology.

The α -Fe and Fe-Co powders used in this method were commercial powders of micrometer size. Figure 4 is a SEM micrograph showing α -Fe powder particles used in this research project. The powder particles are spheres with an average diameter of 3 to 5 micrometers. Figure 5 shows the cross section of a few α -Fe powder particles. It can be seen that each α -Fe particle is comprised of many fine grains with the grain size in the nanometer range.

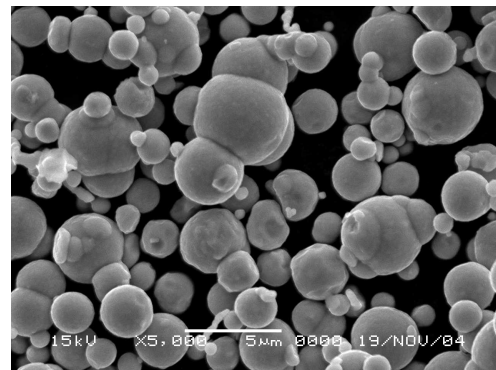


Fig. 4. SEM micrograph of α -Fe powder particles used in this project.

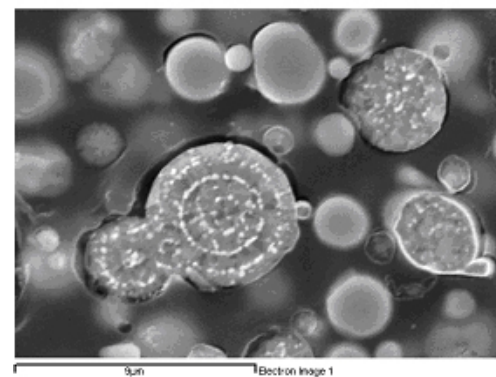


Fig. 5. SEM micrograph of cross section of α -Fe powder particles

Figure 6 shows Fe-Co powder particles used in this research project. Fe-Co powder particles are also spheres but with much larger diameters. The diameter of most Fe-Co particles ranges from 10 to 50 micrometers, although particles of only a few

micrometers are also present. A SEM micrograph of a fracture surface of a Fe-Co particle is shown in Figure 7. Similar to the α -Fe particles, the Fe-Co particles also have nanograin structure. In order to make composite magnets, the α -Fe or Fe-Co powder was blended with the melt-spun Nd-rich $\text{Nd}_{13.5}\text{Fe}_{80}\text{Ga}_{0.5}\text{B}_6$ powder before hot compaction.



Fig. 6. SEM micrograph of Fe-Co powder particles used in this study

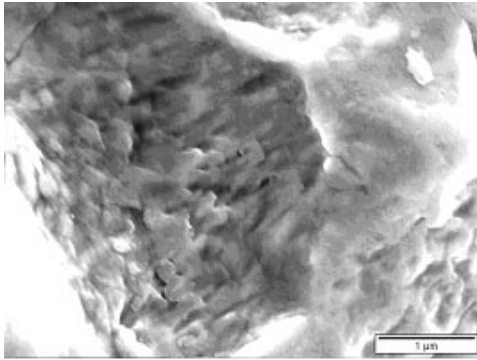


Fig. 7. SEM micrograph of a fracture surface of a Fe-Co particle.

Figure 8 is a SEM backscattered electron image of a hot deformed $\text{Nd}_{13.5}\text{Fe}_{80}\text{Ga}_{0.5}\text{B}_6/\alpha\text{-Fe}$ (91.7 wt%/8.3 wt%) magnet. The dark gray phase is the α -Fe, while the light gray is the Nd-Fe-B phase. The length of the α -Fe phase can be up to over 20 micrometers with a thickness of 5 to 10 micrometers. Apparently, the α -Fe powder particles were agglomerated during processing. Unlike the α -Fe particles, the Fe-Co particles were not agglomerated. As shown in Figure 9, each individual Fe-Co phase (the dark gray phase) was formed from a single Fe-Co particle.

It was a great surprise that both composite $\text{Nd}_{13.5}\text{Fe}_{80}\text{Ga}_{0.5}\text{B}_6/\alpha\text{-Fe}$ and $\text{Nd}_{13.5}\text{Fe}_{80}\text{Ga}_{0.5}\text{B}_6/\text{Fe-Co}$ magnets demonstrated very smooth demagnetization curves with moderately high M_Hc

of over 10 kOe and $(BH)_{\text{max}}$ up to ~ 50 MGOe, as shown in Figures 10 and 11, respectively. The specimen shown in Figure 9 has $M_Hc = 10.2$ kOe and $(BH)_{\text{max}} = 46$ MGOe. In comparison, the typical magnetic properties of the annealed $\text{Nd}_{13.5}\text{Fe}_{80}\text{Ga}_{0.5}\text{B}_6$ powder were $B_r \approx 8$ kG, $M_Hc \approx 17$ kOe, and $(BH)_{\text{max}} \approx 15$ MGOe.

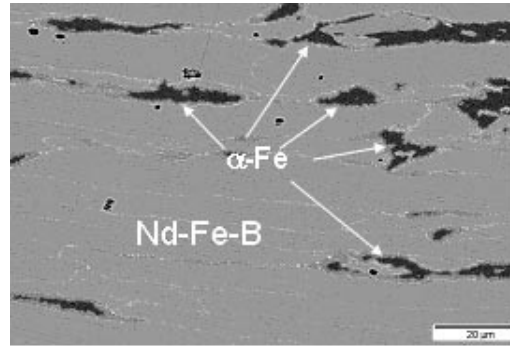


Fig. 8. SEM backscattered electron image of a hot deformed composite $\text{Nd}_{13.5}\text{Fe}_{80}\text{Ga}_{0.5}\text{B}_6/\alpha\text{-Fe}$ (91.7 wt%/8.3 wt%) magnet.

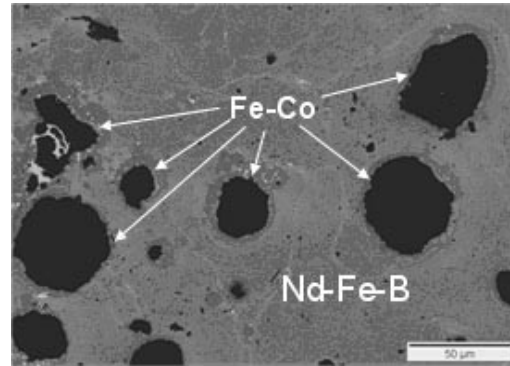


Fig. 9. SEM backscattered electron image of a hot deformed composite $\text{Nd}_{13.5}\text{Fe}_{80}\text{Ga}_{0.5}\text{B}_6/\text{Fe-Co}$ (95 wt%/5 wt%) magnet.

X-ray diffraction (XRD) analyses revealed that using the technique of blending Nd-Fe-B with α -Fe or Fe-Co powder significantly improves grain alignment in composite magnets. Figure 12 compares XRD patterns of three magnets. Better grain alignment is represented by enhanced (004), (006), and (008) intensity and a greater than 1 intensity ratio of (006) over (105). It can be seen that the grain alignment of the magnet prepared using blending α -Fe technique is much better than that of a magnet prepared using blending a Nd-rich alloy and a Nd-poor alloy and similar to that of a commercial sintered anisotropic Nd-Fe-B magnet.

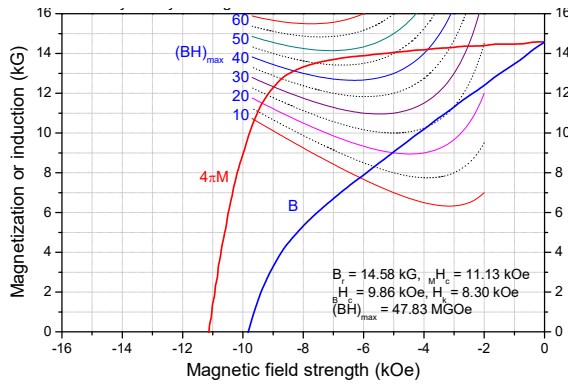


Fig. 10. Demagnetization curves of an anisotropic $\text{Nd}_{13.5}\text{Fe}_{80}\text{Ga}_{0.5}\text{B}_6/\alpha\text{-Fe}$ (95 wt%/5 wt%) magnet.

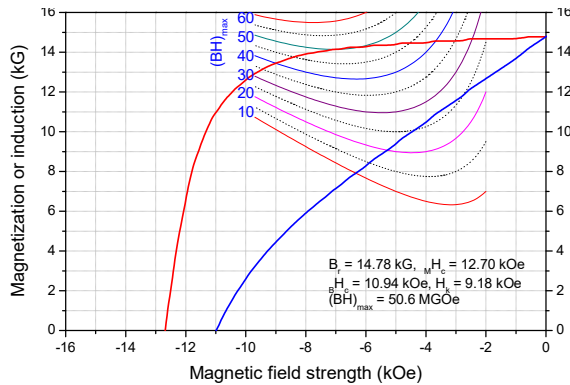


Fig. 11. Demagnetization curves of an anisotropic $\text{Nd}_{13.5}\text{Fe}_{80}\text{Ga}_{0.5}\text{B}_6/\text{Fe-Co}$ (95 wt%/5 wt%) magnet.

Figure 13 shows elongated and aligned nanograins in the 2:14:1 matrix phase of a $\text{Nd}_{13.5}\text{Fe}_{80}\text{Ga}_{0.5}\text{B}_6/\alpha\text{-Fe}$ (95 wt%/5 wt%) magnet with $(\text{BH})_{\text{max}} = 48$ MGOe. It can be seen that the length of some small grains is less than 100 nm, while some large grains are longer than 300 nm. Most grains are well aligned and the grain alignment is much better than that of previously made nanocomposite magnets, such as those described in [18,19].

Figure 14 shows the hard/soft interface of the same specimen. In addition to elongated and aligned nano $\text{Nd}_2\text{Fe}_{14}\text{B}$ grains, as shown in the right-top corner of the figure, large $\text{Nd}_2\text{Fe}_{14}\text{B}$ grains are observed at the interface, while large $\alpha\text{-Fe}$ particles basically maintain their original round shape after hot deformation. Further, the $\alpha\text{-Fe}$ particle demonstrates some detailed fine structure, which excludes it from being a single-grain particle. This is in agreement with what observed in Figure 5.

As expected, adding more soft phase resulted in higher magnetization but lower coercivity. The best magnetic performance was obtained when the $\alpha\text{-Fe}$ or Fe-Co fraction was around 3 to 8%.

Figures 15 and 16 show the effects of the soft $\alpha\text{-Fe}$ content on B_r , M_{Hc} , and $(\text{BH})_{\text{max}}$ of nanocomposite $\text{Nd-Fe-B}/\alpha\text{-Fe}$ magnets, respectively. Increasing the $\alpha\text{-Fe}$ fraction in the composite magnets results in gradually enhanced B_r , but decreased M_{Hc} , as shown in Figure 15. These two conflicting factors led to a peak of $(\text{BH})_{\text{max}}$ at around 5% $\alpha\text{-Fe}$ as shown in Figure 16.

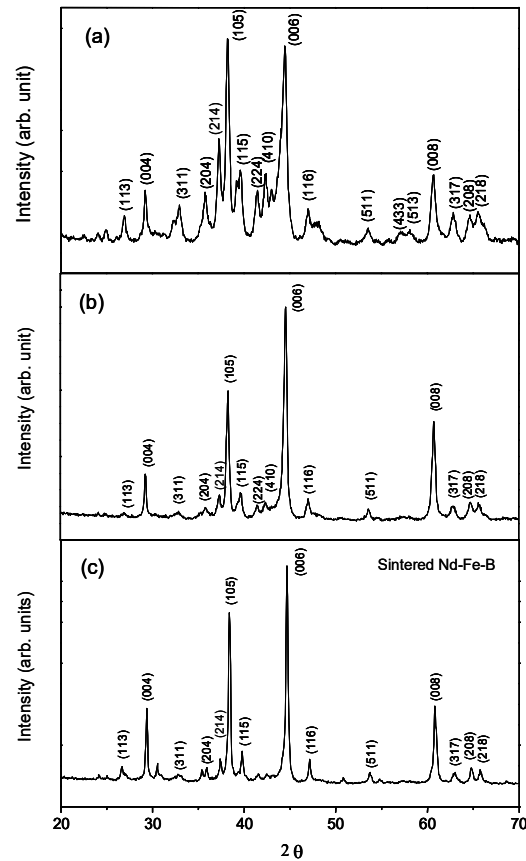


Fig. 12. A comparison of XRD patterns of (a) a composite $\text{Nd}_2\text{Fe}_{14}\text{B}/\alpha\text{-Fe}$ magnet with $(\text{BH})_{\text{max}} \sim 40$ MGOe prepared by blending a Nd-rich Nd-Fe-B powder with a Nd-poor Nd-Fe-B powder, (b) a composite $\text{Nd-Fe-B}/\alpha\text{-Fe}$ magnet with $(\text{BH})_{\text{max}} \sim 50$ MGOe prepared by blending a Nd-rich Nd-Fe-B powder with an $\alpha\text{-Fe}$ powder, and (c) a commercial sintered Nd-Fe-B magnet with $(\text{BH})_{\text{max}} \sim 40$ MGOe.

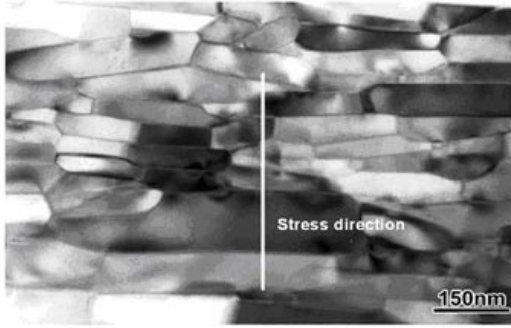


Fig. 13. TEM micrograph of the $\text{Nd}_2\text{Fe}_{14}\text{B}$ matrix phase of a composite Nd-Fe-B/ α -Fe magnet prepared by blending a Nd-Fe-B powder with an α -Fe powder.

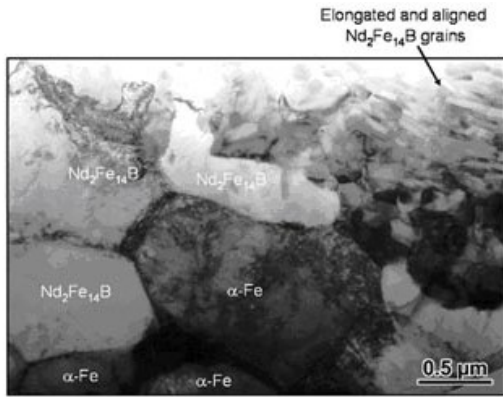


Fig. 14. TEM micrograph of the hard/soft interface of a composite Nd-Fe-B/ α -Fe magnet prepared by blending a Nd-Fe-B powder with an α -Fe powder.

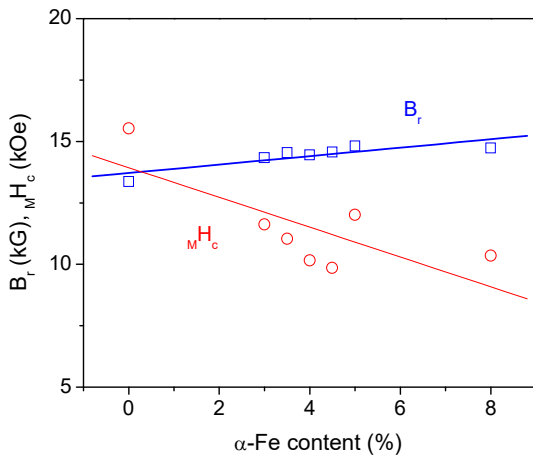


Fig. 15. Effect of α -Fe content on B_r and MH_c of nanocomposite $\text{Nd}_2\text{Fe}_{14}\text{B}/\alpha$ -Fe magnets.

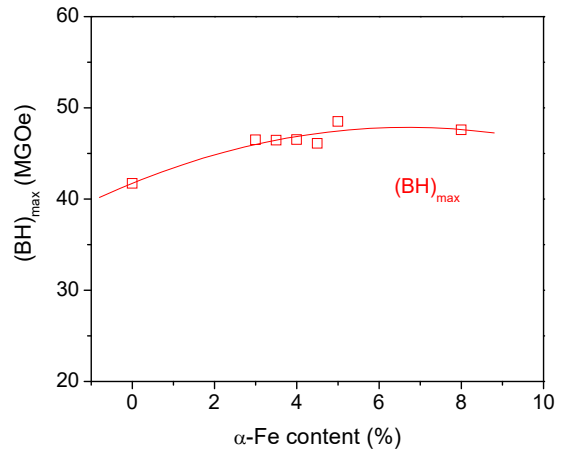


Fig. 16. Effect of α -Fe content on $(BH)_{max}$ of nanocomposite $\text{Nd}_2\text{Fe}_{14}\text{B}/\alpha$ -Fe magnets.

Figures 17 and 18 show the effect of the Fe-Co fraction on the magnetic properties of composite $\text{Nd}_{13.5}\text{Fe}_{80}\text{Ga}_{0.5}\text{B}_6/\text{Fe-Co}$ magnets. With increasing Fe-Co content, B_r increases from around 13 kG when the Fe-Co content is 0 to around 15 kG when the Fe-Co content is 9%. At the same time, MH_c decreases from over 15 kOe to around 8 kOe, as shown in Figure 17. As shown in Figure 18, a peak of $(BH)_{max}$ near 48 MGOe appears when the Fe-Co content is around 4%.

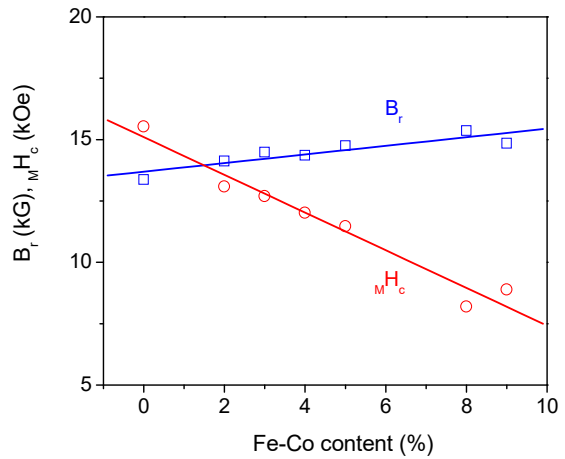


Fig. 17. Effects of Fe-Co fraction on B_r and MH_c of composite $\text{Nd}_{13.5}\text{Fe}_{80}\text{Ga}_{0.5}\text{B}_6/\text{Fe-Co}$ magnets.

Previous studies [3-5] reported that the optimum size of the soft phase in a composite Nd-Fe-B/ α -Fe magnet is ~ 10 nm and its upper limit is approximately 20 – 30 nm for effective interface exchange coupling. However, this study

demonstrates that smooth demagnetization curves and high magnetic performance up to 50 MGOe can be obtained even when the soft phase has a very large size up to 40 micrometers. This soft phase dimension is more than 1000 times larger than the upper limit of the soft phase size suggested in the current models of interface exchange coupling. This indicates that the hard/soft interface exchange coupling in a composite magnet is actually much stronger than what investigators previously understood.

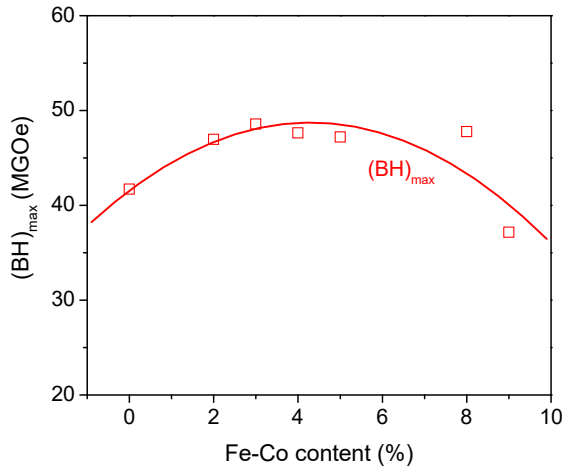


Fig. 18. Effects of Fe-Co fraction on $(BH)_{max}$ of composite $Nd_{13.5}Fe_{80}Ga_{0.5}B_6/Fe-Co$ magnets.

4.4 Hot compaction and hot deformation of Nd-rich Nd-Fe-B powder particles coated with α -Fe or Fe-Co layers

The magnetically soft phase can be very large (up to tens of micrometers), as described previously. However, this does not mean that a large soft phase benefits magnetic properties of a composite magnet. Actually, a very fine and highly dispersed soft phase uniformly distributed in a nanograin hard matrix will tremendously increase the total area of the hard/soft interface and, thus will result in more effective interface exchange coupling between the two phases, which will make it possible for more soft phase to be added into the composite magnets and will lead to significantly improved magnetic performance. Therefore, the microstructures shown in Figures 8 and 9 are by no means desirable.

In order to significantly decrease the size and improve the distribution of the soft phase, a new approach has been applied to make nanograin composite magnets by coating the melt-spun Nd-rich Nd-Fe-B powder particles with thin layers of

α -Fe or Fe-Co followed by normal hot compaction and hot deformation. The coating technologies that have been used include sputtering, pulsed laser deposition (PLD), chemical (electroless) coating, and electrolytic coating.

4.4.1 Composite magnets prepared by using sputtering and pulsed laser deposition techniques

Both sputtering and PLD were used to coat Nd-Fe-B powders. The target used was an α -Fe metal or an Fe-Co-V alloy (Hipercor 50). A rotating powder sample holder was used to obtain more uniform coated layers. The sputtering was performed under Ar atmosphere with a chamber pressure of 15 mtorr. For PLD, Nd:Y₃Al₅O₁₂ ($\lambda = 1064$ nm) laser was used with 340 mJ/pulse and 10 Hz. The chamber pressure was 10^{-5} Pa. For both sputtering and PLD, the deposition time varied from 15 minutes up to 21 hours.

The SEM observations showed that in most cases, the coated layers were not smooth and uniform, but had rough and mottled morphology as shown in Figure 19.

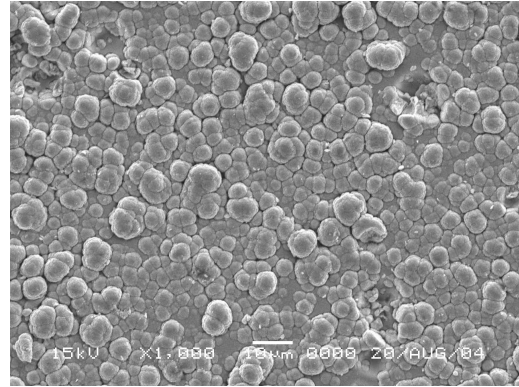


Fig. 19. A SEM micrograph of a coated surface of a Nd-Fe-B powder particle after DC sputtering for 20 hours.

Nanograin composite magnets prepared using sputtering and PLD techniques demonstrated increased intrinsic coercivity and significantly improved loop squareness as specified by the high knee field value. Figure 20 shows demagnetization curves of a nanograin composite $Nd_{14}Fe_{79.5}Ga_{0.5}B_6/Fe-Co$ magnet prepared using DC sputtering for 21 hours.

Another advantage of using sputtering and PLD is their low oxygen pickup. After the deposition, the oxygen content of the coated powder ranges from 0.04 to 0.06 wt%, almost in the same level as the original uncoated powder.

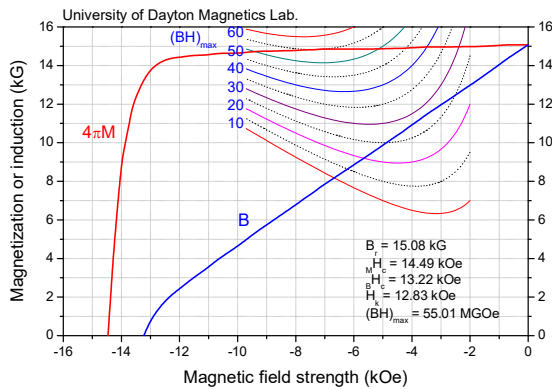


Fig. 20. Demagnetization curves of a composite $\text{Nd}_{14}\text{Fe}_{79.5}\text{Ga}_{0.5}\text{B}_6/\text{Fe-Co}$ magnet prepared using DC sputtering for 21 hours

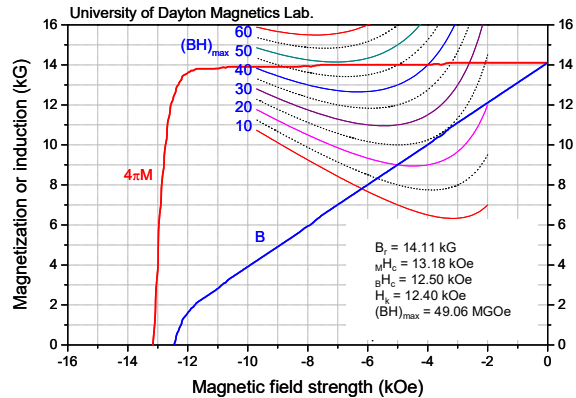


Fig. 21. Demagnetization curves of a composite $\text{Nd}_{14}\text{Fe}_{79.5}\text{Ga}_{0.5}\text{B}_6/\text{Fe-Co}$ magnet prepared using chemical coating for 1 hour with $(\text{BH})_{\text{max}} = 49.06 \text{ MGOe}$.

4.4.2 Composite magnets prepared by using chemical coating technique

Both sputtering and PLD are time-consuming processes with high cost. Therefore, chemical (electroless) coating was used to coat Nd-Fe-B powder particles. The advantage of the chemical coating includes shorter coating time, lower cost, and more controllable process parameters.

For chemical coating, a solution of $\text{FeSO}_4 \cdot 7\text{H}_2\text{O}$ and $\text{CoSO}_4 \cdot 7\text{H}_2\text{O}$ at 0.1 mol/l, respectively, was used as the solute, with $\text{NaH}_2\text{PO}_2 \cdot \text{H}_2\text{O}$ at 0.4 mol/l added as a reducing agent and $\text{Na}_3\text{C}_6\text{H}_5\text{O}_7 \cdot 2\text{H}_2\text{O}$ at 0.3 mol/l added as a complexing agent. The solution pH value was 5 to 8, the temperature was 20 to 50 °C, and the coating time was from 15 minutes to 2 hours.

Figure 21 shows demagnetization curves of a $\text{Nd}_{14}\text{Fe}_{79.5}\text{Ga}_{0.5}\text{B}_6/\text{Fe-Co}$ magnet prepared using chemical coating for 1 hour at room temperature.

It was a surprise that low oxygen pick up also associated with the chemical coating process, even a water solution was used. Coating at elevated temperature resulted in increased deposition rate and, hence, enhanced magnetization, but deteriorated coercivity as a result of more oxygen pickup.

4.4.3 Composite magnets prepared by using electrolytic coating technique

It was observed that the deposition rate of the chemical Fe-Co or $\alpha\text{-Fe}$ coating is slow. Further, only about one-fourth to one-third of the powder particles could be coated with Fe-Co or $\alpha\text{-Fe}$ layers. Most powder particles could not be coated with any soft magnetic material. To significantly increase the coating rate, the feasibility of applying electrolytic coating was investigated.

For electrolytic coating, the solute used were $\text{FeSO}_4 \cdot 7\text{H}_2\text{O}$ and $\text{CoSO}_4 \cdot 7\text{H}_2\text{O}$ at 0.3 mol/l with an addition of $\text{MgSO}_4 \cdot 7\text{H}_2\text{O}$ at 0.3 mol/l. The solution pH value was 2 to 3, the temperature was 25 to 30°C, and the coating time was 15 minutes to 2 hours. The anode and cathode materials were Fe-Co and aluminum, respectively. The cathode current density was 0.5 to 5 A/dm^2 .

The electrolytic coating was found to have greater deposition rate than the chemical coating. However, if the coating layer is too thick, it turns to be peeled off from the ribbon surface. Figure 22 shows a SEM micrograph of Nd-Fe-B ribbons coated using electrolyte coating for 1 hour. From the morphology of the coated Fe-Co layer at high magnification, such as shown in Figure 23, it is believed that the coated Fe-Co is in an amorphous condition.

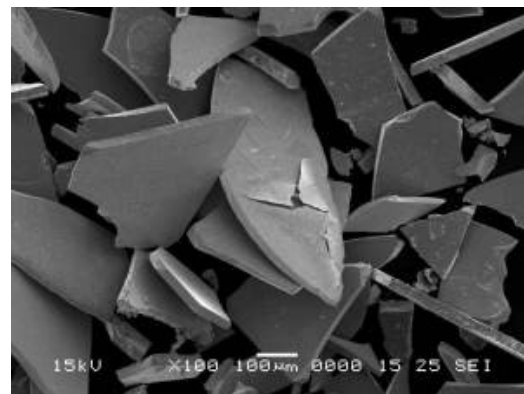


Fig. 22. SEM micrograph of ribbons coated by electrolytic coating for 1 hour.

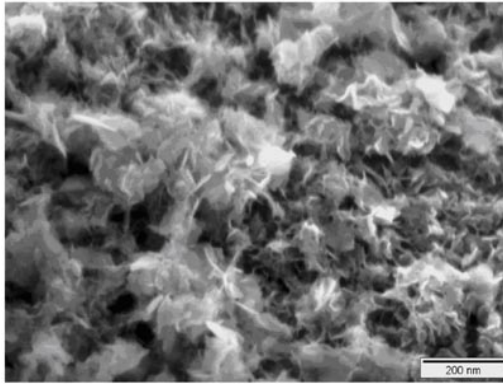


Fig. 23. High-resolution SEM micrograph of the coated surface of an Nd-Fe-B powder particle after electrolytic coating for 1 hour.

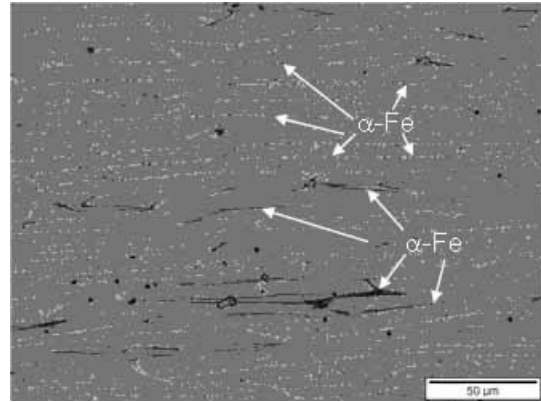


Fig. 25. SEM micrograph of a composite $\text{Nd}_{14}\text{Fe}_{79.5}\text{Ga}_{0.5}\text{B}_6/\alpha\text{-Fe}$ magnet prepared using electrolytic coating.

Figure 24 illustrates demagnetization curves of a composite $\text{Nd}_{14}\text{Fe}_{79.5}\text{Ga}_{0.5}\text{B}_6/\alpha\text{-Fe}$ magnet prepared using electrolyte coating for 30 minutes under 2 volts and 1 ampere. Because magnets prepared using electrolyte coating have a relatively high oxygen content ranging from 0.1 to 0.3 wt%, these magnets demonstrate relatively low M_Hc .

Figure 25 shows a SEM micrograph of a composite $\text{Nd}_{14}\text{Fe}_{79.5}\text{Ga}_{0.5}\text{B}_6/\alpha\text{-Fe}$ magnet prepared using electrolytic coating. In addition to the matrix Nd-Fe-B phase, the corresponding EDS (Figure 26) identified a $\alpha\text{-Fe}$ phase (the black phase in Figure 25) and a Nd- and oxygen-rich phase (the white phase in Figure 25).

Figure 27 shows a TEM micrograph of a specimen cut parallel to the deformation direction, showing the elongated and aligned grains of the

matrix phase in an $\text{Nd}_{14}\text{Fe}_{79.5}\text{Ga}_{0.5}\text{B}_6/\alpha\text{-Fe}$ magnet prepared by electrolytic coating for 1 hour. The elongated grains have a thickness of about 100 to 200 nm and length of a few hundred nanometers. Some large grains were also observed. With further reduction of the grain size through optimized processing, magnetic performance, especially coercivity, can be significantly improved.

Figure 28 illustrates the minor Nd-rich phase, identified by TEM/EDS analysis, distributed at the grain boundaries of $\text{Nd}_2\text{Fe}_{14}\text{B}$ grains.

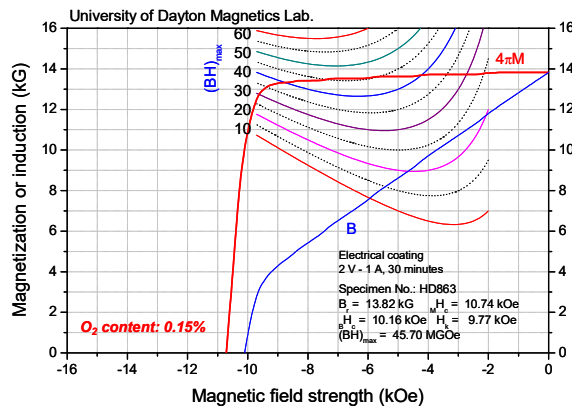


Fig. 24. Demagnetization curves of a composite $\text{Nd}_{14}\text{Fe}_{79.5}\text{Ga}_{0.5}\text{B}_6/\alpha\text{-Fe}$ magnet prepared using electrolytic coating for 30 minutes.

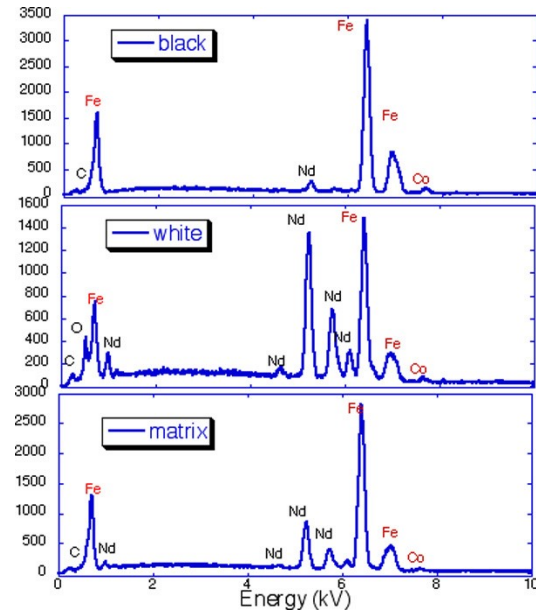


Fig. 26. SEM/EDS of a composite $\text{Nd}_{14}\text{Fe}_{79.5}\text{Ga}_{0.5}\text{B}_6/\alpha\text{-Fe}$ magnet prepared using electrolytic coating.

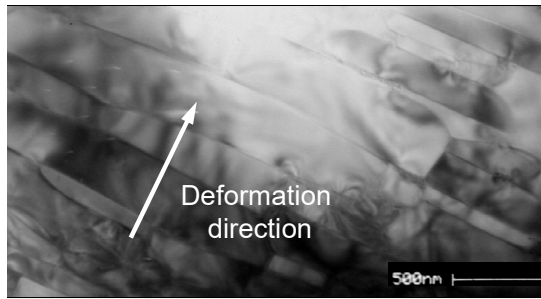


Fig. 27. TEM micrograph of the $\text{Nd}_2\text{Fe}_{14}\text{B}$ phase of an $\text{Nd}_{14}\text{Fe}_{79.5}\text{Ga}_{0.5}\text{B}_6/\alpha\text{-Fe}$ magnet prepared using electrolytic coating.

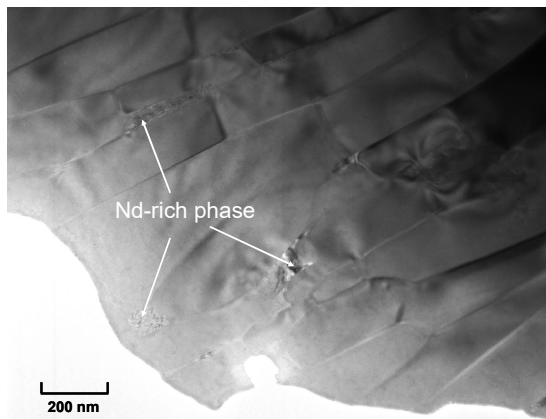


Fig. 28. TEM micrograph showing the Nd-rich phase, identified by TEM/EDS, at grain boundaries of $\text{Nd}_2\text{Fe}_{14}\text{B}$ grains.

Figure 29 is a selected area electron diffraction pattern of a $\text{Nd}_{14}\text{Fe}_{79.5}\text{Ga}_{0.5}\text{B}_6/\alpha\text{-Fe}$ magnet prepared using electrolytic coating for 1 hour and cut perpendicular to the deformation direction, showing crystallographic direction [001] of tetragonal $\text{Nd}_2\text{Fe}_{14}\text{B}$ superimposed with rings of amorphous or very fine grains of body-centered-cubic $\alpha\text{-Fe}$. The existence of an amorphous phase after exposure to an elevated temperature of around 900°C for a short period of time was also observed in previous experiments.

Synthesizing bulk anisotropic nanograin composite magnets by utilizing powder blending and powder coating technologies is still in its very early stage of development. A better powder blending technology is yet to be developed in which fine (preferred to be in nanometer range) $\alpha\text{-Fe}$ or Fe-Co powder can be uniformly blended with Nd-Fe-B powder without oxidation and agglomeration.

Similarly, a better coating technology with an improved deposition rate and lower oxygen pickup is yet to be developed. However, the powder coating approach is one step forward toward

creating a desired microstructure, i.e. a highly dispersed magnetically soft phase, such as $\alpha\text{-Fe}$ or Fe-Co , is uniformly distributed in a nanograin magnetically hard phase, such as Nd-Fe-B .

Adding a magnetically soft phase into Nd-Fe-B certainly enhances its magnetization, but decreases its coercivity. However, it is important to note that the reduction of the coercivity depends not only on the amount of the soft phase added, but also very strongly depends on the size and distribution of the soft phase. A very fine and highly dispersed soft phase will result in a very large hard/soft interfacial area, thus, leading to a more effective hard/soft interface exchange coupling, which will minimize the reduction in coercivity. In addition, this effect will allow more magnetically soft phase to be accommodated in a composite magnet, leading to higher magnetization and enhanced magnetic performance.

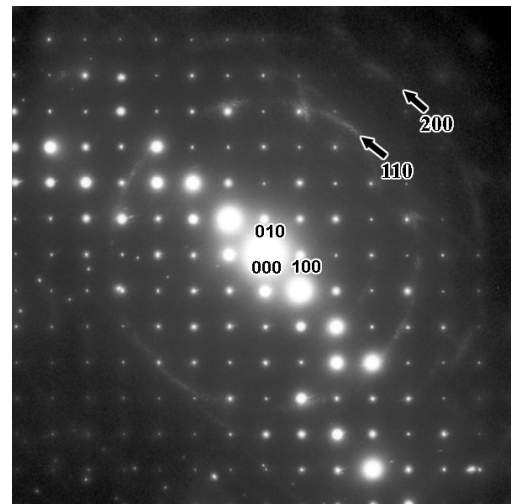


Fig. 29. Selected area electron diffraction of a perpendicular section of an $\text{Nd}_{14}\text{Fe}_{79.5}\text{Ga}_{0.5}\text{B}_6/\alpha\text{-Fe}$ magnet prepared using electrolytic coating.

5. Conclusions

- An innovative rapid inductive hot compaction technique was developed. Using this technology, melt-spun or mechanically alloyed nanocomposite rare earth alloy powders can be made into bulk magnets with full density even when the rare earth content is as low as 4 at%.
- Innovative powder blending technique and powder coating techniques were developed. Applying these techniques, bulk anisotropic nanograin composite $\text{Nd-Fe-B}/\alpha\text{-Fe}$ or $\text{Nd-Fe-B}/\text{Fe-Co}$ magnets with good nanograin alignment can be synthesized. The $(\text{BH})_{\text{max}}$ of these composite magnets were 40 to 55 MGOe. Much higher magnetic performance is

anticipated with further reductions in the size and improvements in the distribution of the magnetically soft phase.

- It was observed that the magnetically soft phase in a composite magnet can be as large as up to 40 micrometers. This soft phase size is more than 1000 times larger than the upper limit of the soft phase size suggested in the current models of interface exchange coupling in nanocomposite magnet materials.

References:

- [1] Buschow, K.H.J. de Mooij, D.B. and Coehoorn, R., "Metastable Ferromagnetic Materials for Permanent Magnets," *J. Less-Common Metals*, 1988, 145, 601-611.
- [2] Coehoorn, R., de Mooij, D. B., and de Waard, C., "Melt Spun Permanent Magnets Materials Containing Fe₃B as the Main Phase," *J. Magn. Magn. Mater.*, 1989, 80, 101.
- [3] Kneller, E.F. and Hawig, R., "The Exchange-Spring Magnet: A New Material Principle for Permanent Magnets," *IEEE Trans. Magn.*, 1991, 27, 3588.
- [4] Wecker, J. Katter, M., and Schultz, L., "Mechanically Alloyed Sm-Co Materials," *J. Appl. Phys.*, 1991, 69, 6058.
- [5] Manaf, A. Buckley, R.A., and Davies, H.A., "New nanocrystalline high-remanence Nd-Fe-B alloys by rapid solidification," *J. Magn. Magn. Mater.*, 1993, 128, 302.
- [6] Skomski, R. and Coey, J.M.D., "Giant Energy product in nanostructured two-phase magnets," *Phys. Rev. B*, 1993, 48, 15812.
- [7] Chen, Z. Zhang, Y. Daniil, M. Okumura, H. Hadjipanayis, G.C., and Chen, Q., "Review of Rare Earth Nanocomposite Magnets," *Proc. of the 16th Int'l Workshop on REM*, vol.1, 449, 2000.
- [8] Croat, J.J., "Current Status of Rapidly Solidified Nd-Fe-B Permanent Magnets," *Proc. of the 11th Int'l Workshop on REM*, ed. S.G. Sankar, vol. 1, p. 1, 1990.
- [9] Senno H. and Tawara, Y., "Permanent-Magnet Properties of Sm-Ce-Co-Fe-Cu Alloys with Compositions Between 1-5 and 2-17," *IEEE Trans. Magn.*, 1974, 10, 313.
- [10] Ojima, T., Tomizawa, S., Yoneyama, T., and Hori, T., "Magnetic Properties of a New Type of Rare-Earth Cobalt Magnets Sm₂(Co, Cu, Fe, M)₁₇," *IEEE Trans. Magn.*, 1977, 1, 1317
- [11] Ray, A.E., "The development of high energy product permanent magnets from 2:17 RE-TM alloys," *IEEE Trans. Magn.*, 1984, 20, 1615.
- [12] Ray, A.E. Soffa, W.A., Blachere, J.R., and Zhang, B., "Cellular Microstructure Development in Sm(Co,Fe,Cu,Zr)_{8.35} Alloys," *IEEE Trans. Magn.*, 1987, 23, 2711.
- [13] Ray, A.E., and Liu, S., "Recent progress in 2:17 type permanent magnets," *J. Material Engineering and Performance*, 1992, 1, 183-192.
- [14] Chen, S.K., Tsai, J.L., and Chin, T.S., "Nanocomposite Sm₂Co₁₇/Co permanent magnets by mechanical alloying," *J. Appl. Phys.*, 1996, 79, 5964.
- [15] Cui, B.Z., Huang, M.-Q., and Liu, S., "Magnetic Properties of SmCo₇/Co and Sm(Co,Fe)₇ α-(Fe,Co) Nanocomposite Magnets Prepared by Magnetic Annealing," *IEEE Trans. Magn.*, 2003, 39, 2866.
- [16] Liu, S., "Effect of Nanograin Structure on Magnetic Properties of Rare Earth Permanent Magnets," *Proc. of the 18th Workshop on HPM*, vol. 2, 690, 2004.
- [17] Liu, S., Cui, B., Bauser, S., Leese, R., Hilton, J.S., Yu, R.H., Kramp, A., Dent, J., and Miles, D., "Approach to synthesizing bulk, fully dense anisotropic nanocomposite rare earth permanent magnets," *Proc. of the 17th Int'l. Workshop on REPM*, 939, 2002.
- [18] Lee, D., Hilton, J.S., Liu, S., Zhang, Y., Hadjipanayis, G.C., and Chen, C.H., "Hot pressed and hot deformed (Nd,Pr,Dy)₂Fe₁₄B/α-Fe based nanocomposite magnets," *IEEE Trans. on Magn.*, 2003, 39, 2947.
- [19] Lee, D., Hilton, J.S., Chen, C.H., Huang, M.Q., Zhang, Y., Hadjipanayis, G.C., and Liu, S., "Bulk Isotropic and Anisotropic Rare Earth Magnets," *IEEE Trans. Magn.*, 2004, 40, 2004.